Environmental Science: Atmospheres

ROYAL SOCIETY OF CHEMISTRY

PAPER

View Article Online
View Journal

Check for updates

Cite this: DOI: 10.1039/d5ea00128e

Seven years of measurements of equivalent black carbon at the Capo Granitola WMO-GAW station: influence of local vegetation fires

Salvatore Sodano, †*[a] Stefania Gilardoni, [b] Angela Marinoni, [a] Tony C. Landi, [a] Davide Putero, [c] Giorgio Tranchida, [d] Luca Di Liberto [e] and Paolo Bonasoni [f]

This study investigates the influence of local vegetation fires on equivalent black carbon (eBC) concentrations using seven years of satellite and ground-based observations combined with HYSPLIT back-trajectory analysis. Measurements were collected at the 'Rita Atria' Climate Observatory at Capo Granitola (CGR), a WMO-GAW background-coastal regional station located on the south-west coast of Sicily in the central Mediterranean Basin. Between 2015 and 2021, the Sicilian region experienced approximately 6330 vegetation fires, with 74% occurring during the summer season. The total burned area amounted to 135 thousand hectares (ha), with roughly 30% being forested land, averaging about 6.1 kha per year, and 67% affecting other types of vegetation. The average eBC concentration was 0.49 ± 0.69 μg m^{-3}, with significant interannual variability. 10% of the days were characterized by eBC concentrations exceeding the climatological average, referred to as acute days. Using back-trajectory analysis, vegetation fire influence on acute eBC days was evaluated using satellite-based MODIS/VIIRS active-fire pixels and ground-based burned areas from the Sicilian Forest Information System (SIF). We found matches for 46% and 18% of acute days, respectively, consistent with the different nature and coverage of the two products. A statistically significant increasing trend of eBC concentration during the acute days was observed (0.04 μg m^{-3} per year), consistent with an increase in the frequency of vegetation fires, highlighting the intensifying impact of these events on air quality in the central Mediterranean.

Received 30th September 2025
Accepted 3rd March 2026

DOI: 10.1039/d5ea00128e

rsc.li/esatmospheres

Open Access Article. Published on 07 April 2026. Downloaded on 4/13/2026 10:22:05 AM.
This article is licensed under a Creative Commons Attribution-NonCommercial 3.0 Unported Licence.

Environmental significance

Vegetation fires are increasingly recognized as a significant source of atmospheric pollutants. The present investigation reports an increase in equivalent black carbon (eBC) concentrations associated with a local vegetation fire event. Furthermore, it provides the scientific community with the first measurements of eBC levels in this area, thereby addressing an important knowledge gap. These data also contribute to a more consistent understanding of eBC dynamics across the Mediterranean region, offering a broader perspective on the role of biomass burning in shaping atmospheric composition. Overall, our findings demonstrate that local air quality is particularly vulnerable to climate-driven fire activity and provide actionable evidence for regional environmental managers and policymakers to strengthen fire prevention strategies and mitigate impacts on ecosystems and public health.

1 Introduction

Black carbon (BC) is a highly light-absorbing component of carbonaceous aerosols that influences the atmospheric energy balance and acts as a climate forcer,[1] also posing a significant threat to human health.[2] BC is produced by the incomplete combustion of fossil fuels and biofuels, such as diesel, coal and wood,[3] and is often called "soot".[4,5] BC is a short-lived climate forcer (SLCF), with an atmospheric lifetime of 4–12 days;[3,6,7] both its residence time and its direct and indirect climate impacts depend on mixing with other aerosol components and meteorological conditions.[8] Open burning dominates BC emissions on a global scale[9] and, in some regions, accounts for

[a]Institute of Atmospheric Sciences and Climate, National Research Council of Italy, Bologna, Italy. E-mail: salvatore.sodano@utas.edu.au
[b]Institute of Polar Sciences, National Research Council of Italy, Milan, Italy
[c]Institute of Atmospheric Sciences and Climate, National Research Council of Italy, Turin, Italy
[d]Institute for the Study of Anthropic Impacts and Sustainability in Marine Environment, National Research Council of Italy, Capo Granitola, Italy
[e]Institute of Atmospheric Sciences and Climate, National Research Council of Italy, Rome, Italy
[f]PROAMBIENTE Tecnopolo CNR, Bologna, Italy
† Present address: Institute for Marine and Antarctic Studies, University of Tasmania, Hobart, Australia.

Open Access Article. Published on 07 April 2026. Downloaded on 4/13/2026 10:22:05 AM.
This article is licensed under a Creative Commons Attribution-NonCommercial 3.0 Unported Licence.

more than 50% of total emissions. Several studies show that climate change promotes drought in multiple areas of the globe, potentially increasing the frequency and severity of fires and consequently increasing BC atmospheric burden, especially in extratropical regions.[10–12] In addition, such climatic conditions can contribute to lengthening the fire season and increasing the number of days with a high fire hazard. In the Euro-Mediterranean basin, where "Mediterranean amplification" (*i.e.* a north–south warming gradient) is active, climate models project both a strong warming and precipitation deficit that will exacerbate fire weather conditions.[13] In the southern regions of the Italian peninsula, located in the heart of the Mediterranean basin, Michetti and Pinar, 2019 (ref. 14), reported a rise in both the frequency of vegetation fires and the extent of burned areas compared to the rest of the country. The need to monitor the impacts of open burning on the atmospheric concentration of climate forcers and atmospheric pollutants, particularly BC, is increasingly critical for quantifying the climate feedback mechanisms triggered by vegetation fires. This study investigates the seasonal and interannual variability of eBC concentrations from 2015 to 2021, providing valuable insights for policymakers and contributing to the scientific understanding of atmospheric dynamics in the area. For the first time, a long-term analysis of eBC concentrations was carried out at the CGR Climate Observatory, located in a previously unexplored region of the Mediterranean basin.

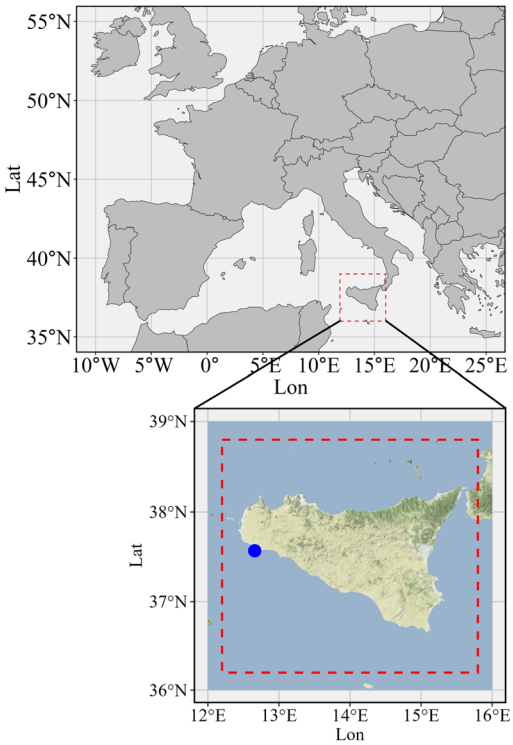

Fig. 1 Top panel: map of Europe highlighting the region of interest for this project (red rectangle); bottom panel: location of the CNR-ISAC observatory 'Rita Atria' at Capo Granitola (blue dot).

2 Measurement site and methodologies

2.1 Sampling site

The measurements were conducted at the "Rita Atria" climate observatory at Capo Granitola (CGR, 37°34′31″N; 12°39′34″E). The observatory is a remote coastal site directly exposed to the Strait of Sicily, making it a strategic location for studying fire emissions in the Mediterranean area, which is one of the regions suffering the most from drought and warming due to climate change.[15,16] The observatory is situated in the southwestern part of Sicily (blue dot in Fig. 1), 11.5 km away from Mazara del Vallo, a town of approximately 50 000 inhabitants that experiences a seasonal tourist fluctuation of about 36%. Established in 2014 and managed by the Institute of Atmospheric Sciences and Climate (CNR-ISAC), the observatory serves as a regional station for the World Meteorological Organization's Global Atmosphere Watch (WMO-GAW) programme. It is a candidate National Facility within the ACTRIS (Aerosols, Clouds and Trace Gases Research Infrastructure) network. The CGR observatory has conducted continuous measurements of aerosol properties (PM, total particle number concentration, BC), reactive gases (O_3, NO, NO_2, and SO_2), greenhouse gases (CH_4, CO, and CO_2), and meteorological parameters throughout its operational history. For the purpose of this study, we focused on the area delimited by the geographic bounding box spanning longitudes 12.2 °E–15.8 °E and latitudes 36.2 °N–38.8 °N (WGS84/EPSG:4326), identified as the local domain covering the Sicily region (Fig. 1).

2.2 *In situ* eBC and meteorological measurements

The eBC concentration is measured continuously with a Multi-Angle Absorption Photometer (MAAP 5012, Thermo Fisher Scientific) with one-minute time resolution, operating at a wavelength of 637 nm with a sample flow rate of 16.7 L min^{-1} downstream of a PM_{10} inlet. The inlet was running under RH controlled conditions as suggested by WMO/ACTRIS guidelines (see the ACTRIS website for further information). The data are processed with automatic routines that perform quality assurance/quality control (QA/QC) actions following the WMO-GAW common data protocol.[17] Absorption by mineral dust can potentially affect the CGR site, particularly during Saharan dust transport events. However, a quantitative assessment of dust absorption was not performed in this study and is beyond the scope of the present paper. Local meteorological parameters (temperature, relative humidity, wind speed and direction, pressure and rain intensity) are measured using a Vaisala Weather Transmitter WXT520. All the measurements, satellite data and other information are reported in local time (LT).

2.3 Satellite and surface observations of vegetation fires

The satellite data used in this study are from the web-based Fire Information for Resource Management System (FIRMS, NASA, https://firms.modaps.eosdis.nasa.gov). In this study we used the Collection 6, version 6.1 MODIS, a sensor capable of identifying active fires, installed on board the Terra (2000 to present) and Aqua (2002 to present) satellites, which fly in the

© 2026 The Author(s). Published by the Royal Society of Chemistry

Open Access Article. Published on 07 April 2026. Downloaded on 4/13/2026 10:22:05 AM. This article is licensed under a Creative Commons Attribution-NonCommercial 3.0 Unported Licence.

polar orbit of the Earth.[18] The product used is the level 3 MOD14/MYD14, with a spatial resolution of 1 km.[19] In addition, the Visible Infrared Imaging Radiometer Suite (VIIRS) sensors installed on board the Suomi National Polar-orbiting Partnership (NPP, 2011) and on NOAA's Joint Polar Satellite System (JPSS, 2017) were considered; these two satellites travel the same orbit separated by 50 minutes and cross the equator 14 times a day, with a spatial resolution of 375 m.[20] The active fires identified by MODIS and VIIRS satellites, which will be referred to as "fire pixels," correspond to the area affected by the active fire. For each fire pixel, the key stored parameters were: (i) latitude and longitude of the center of the pixel; (ii) date and time of acquisition; (iii) confidence value, which for MODIS ranges from 0% to 100% and it was used to assign one of the three confidence classes (low, nominal or high confidence), which instead are already provided for the VIIRS observations; (iv) Fire Radiative Power (FRP), which represents the rate of emitted radiative energy by the fire at the time of the observation; (v) fire type, which provides information on the presumed hot spot type. Four types are identified: 0 = presumed vegetation fire, 1 = active volcano, 2 = other static land source, and 3 = offshore. A filter was applied exclusively to select fire pixels classified as type zero. A detailed description of the listed parameters is reported in Giglio *et al.*, 2016.[19] In addition to satellite observation, we also considered the information from the local registry of surface fires – the Forest Information System (SIF) – build by the Forestry Corps of the Sicilian Region (https://sifweb.regione.sicilia.it/portalsif). The SIF allowed: (i) testing of the accuracy of the satellite observation record; (ii) identification of the type of burnt surface area (*i.e.*, forest and/or non-forest); (iii) definition of a high-resolution map of the area affected by the fires. Therefore, the satellite-derived dataset represents a broader domain of interest, including thermal anomalies with potentially extra-regional origins, whereas the ground-based SIF dataset is restricted to the study region and is available only at regional-scale resolution.

2.4 Back-trajectory analysis

The Hybrid Single-Particle Lagrangian Integrated Trajectory (HYSPLIT[21]) model (see the NOAA website for further information) has been used to trace five-day backward trajectories arriving at CGR during the investigated events. These back-trajectories are used to link the areas where local vegetation fires occurred with the increased concentration of eBC measured at CGR. The model is provided by the National Oceanographic and Atmospheric Administration (NOAA) Air Resources Laboratory (ARL) and the back-trajectories are based on meteorological data from the Global Data Assimilation System (GDAS), with a 1° × 1° horizontal resolution and 23 vertical layers from 1000 to 100 hPa.[22] The method consists in generating a total of 11 back-trajectories, which were calculated around the peak hour of the eBC concentration measured on the acute days (see Section 2.5). Specifically, 5 back-trajectories were created for the five hours prior to the peak, one back-trajectory for the peak hour itself, and another 5 back-trajectories for the five hours following the peak. This approach allows for an in-depth analysis of the atmospheric conditions leading up to, during, and after the peak eBC concentrations and provides more reliability in the prediction of the movement of the air masses. Each trajectory lasts 120 hours and was generated at 100 m a.s.l., above the CGR observatory. For each relevant fire event, the synoptic conditions and wind regimes were additionally evaluated using the non-hydrostatic, fully compressible MOLOCH model[23] to improve representativeness and reduce potential spatial mismatch.

2.5 Definition and analysis of eBC pollution events

The acute eBC days were identified following the methodology reported by Marinoni *et al.*, 2013.[24] Specifically, an acute eBC day was identified when the daily average concentration exceeded the 75th percentile of the climatological baseline distribution. This baseline was obtained through three-time repeated iteration of a centered 21 day running mean applied to daily eBC averages. To ensure measurement representativeness, only days with at least 75% data coverage were considered valid.[25] For each acute eBC day, the hour of maximum daily eBC concentration was identified and used as the central temporal point for back-trajectory calculations (see Section 2.4 for detailed methodology). In order to verify whether these acute eBC days could be attributed to local vegetation fires, we developed a specific source identification algorithm, able to integrate all the available information and characterized by the following inputs:

- The georeferenced information regarding active fire detected by MODIS and VIIRS, during the 5 days before the pollution event.
- The local forest fire archive (SIF), which provides georeferenced information on forest fires in the Sicily region. Each report contains information on the type of fire, geographical location, type of land burned (forest or non-forest), and the start and end dates of the fire.
- The HYSPLIT back-trajectories, lasting 120 hours.

To find correspondence between vegetation fires and acute eBC days, restrictive conditions were defined. In particular, for each point of the back-trajectories, the spatial and temporal correspondence with satellite fire pixels and SIF surface burned areas was verified. To perform this, the following conditions were required:

- Spatial correspondence (x, y, z): a circular area (with a radius of 0.3° ≈ 33.3 km) is traced around the centroid of the satellite fire pixels. The spatial correspondence is verified if at least one point of the back-trajectory transits within such a circular area, and if the altitude of this point is lower than 3000 m a.g.l.;[26]
- Temporal correspondence (t): the back-trajectory point must cross the emission area when the active fire occurs. Because of the satellite overpass time, the correspondence is verified if a fire occurred during the 24 hours prior to the passage of the back-trajectory.

We additionally used the Theil–Sen[27,28] estimator to support the correspondence analysis between acute eBC days and vegetation fires. Statistically, this method estimates the trend

Open Access Article. Published on 07 April 2026. Downloaded on 4/13/2026 10:22:05 AM.
This article is licensed under a Creative Commons Attribution-NonCommercial 3.0 Unported Licence.

Table 1 Statistical summary of seasonal eBC concentrations. (Average) indicates the central tendency of the data – arithmetic mean; (SD) is the standard deviation; (Median) is the middle value; (Q_1) and (Q_3) represent the 25th and 75th percentiles, respectively; (IQR) is the interquartile range calculated as $Q_3 - Q_1$; f_L^T and f_U^T denote the lower and upper fences, defined as $Q_1 - 3 \times$ IQR and $Q_3 + 3 \times$ IQR; (N) is the number of values considered outliers[30]

	Average [μg m^{-3}]	SD [μg m^{-3}]	Median [μg m^{-3}]	Q_3 [μg m^{-3}]	Q_1 [μg m^{-3}]	IQR [μg m^{-3}]	f_L^T [μg m^{-3}]	f_U^T [μg m^{-3}]	N [n]
FALL	0.49	0.47	0.37	0.58	0.21	0.37	0.10	0.69	503
SPRING	0.41	0.37	0.34	0.52	0.20	0.32	0.04	0.69	583
SUMMER	0.70	1.21	0.47	0.78	0.28	0.50	−0.22	1.28	689
WINTER	0.42	0.46	0.31	0.52	0.17	0.35	−0.16	0.85	658

slope as the median of slopes computed from all pairwise combinations of observations, which makes it non-parametric and markedly less sensitive to outliers.

3 Results

3.1 eBC long-term observation and short-term variability

In order to guarantee dataset representativeness, only years with at least 60% of daily data coverage were considered.[29] For this reason, the year 2019, which consisted of 36% of the data, was excluded from the annual statistical analysis. Overall, we collected 45 652 hourly measurements of eBC concentration, corresponding to 1987 measurement days.

Based on continuous measurements collected at the CGR Observatory, the average annual concentration of eBC over the study period was 0.49 ± 0.69 μg m^{-3}, with a maximum recorded in 2020 (0.63 ± 0.92 μg m^{-3}) and the minimum in 2017 (0.42 ± 0.44 μg m^{-3}). Analyzing Table 1, the seasonality of eBC appears moderate, as median values vary within a relatively narrow range across seasons. In summer, the mean and median are approximately 1.67 and 1.52 times higher than in winter, respectively. Summer also shows much more extreme peaks (larger variability and a higher upper fence), while winter features lower typical values but still includes several high episodes.

Fig. 2 illustrates the annual cycle of eBC at monthly resolution. Consistent throughout the years, the summer months (June, July and August, JJA) are characterized by the highest monthly averages and show a larger interannual variability with respect to the other months. The highest monthly eBC concentrations were recorded in August 2020 and 2021 (0.96 ± 1.54 μg m^{-3} and 1.40 ± 3.16 μg m^{-3}, respectively). The lowest concentrations were registered in October 2020 and January 2021 (0.41 ± 0.40 μg m^{-3} and 0.35 ± 0.28 μg m^{-3}, respectively).

The average annual eBC concentration obtained at CGR is comparable to that of Mediterranean coastal background sites such as Finokalia, Greece (0.22 μg m^{-3} EC) and Toulon, France (0.64 ± 0.40 μg m^{-3} eBC), but substantially lower than that at urban Mediterranean sites such as Granada (1.90 ± 2.00 μg m^{-3} eBC) and Athens (1.70 ± 2.20 μg m^{-3} eBC), where traffic and residential wood burning significantly contribute to eBC levels. Vegetation fires have been identified as episodic sources of eBC at Mediterranean sites, particularly during summer, with residential wood combustion contributing 15–30% to eBC in Mediterranean urban areas during winter.[31–35]

3.2 Statistical analysis of acute eBC days

In the period 2015–2021, a total of 198 acute eBC days were identified (see Section 2.5 for the identification methodology), corresponding to 10% of all days in the period (Fig. 3). The highest number of acute eBC days was recorded in 2020 (71 days, corresponding to 35.8% of the total), while the lowest occurred in 2016 (1 day) likely due to limited data availability during winter, when the concentrations are typically highest. On a seasonal scale, we observed that the acute days of eBC occur more frequently in winter (DJF; 59 days, 29.8%), followed by summer (JJA; 50 days, 25.3%), autumn (SON; 49 days, 24.7%), and spring (MAM; 40 days, 20.2%). This pattern is likely attributable to increased fossil fuel combustion for heating

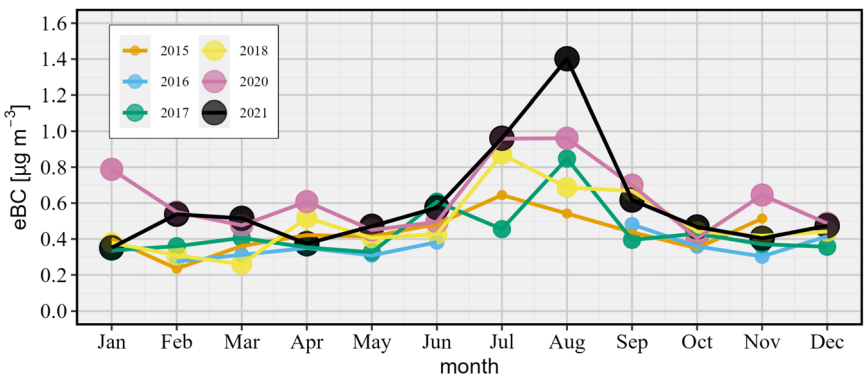

Fig. 2 Monthly eBC concentration for the different years considered in this study. The size of the dots varies according to the year.

© 2026 The Author(s). Published by the Royal Society of Chemistry

Open Access Article. Published on 07 April 2026. Downloaded on 4/13/2026 10:22:05 AM.
This article is licensed under a Creative Commons Attribution-NonCommercial 3.0 Unported Licence.

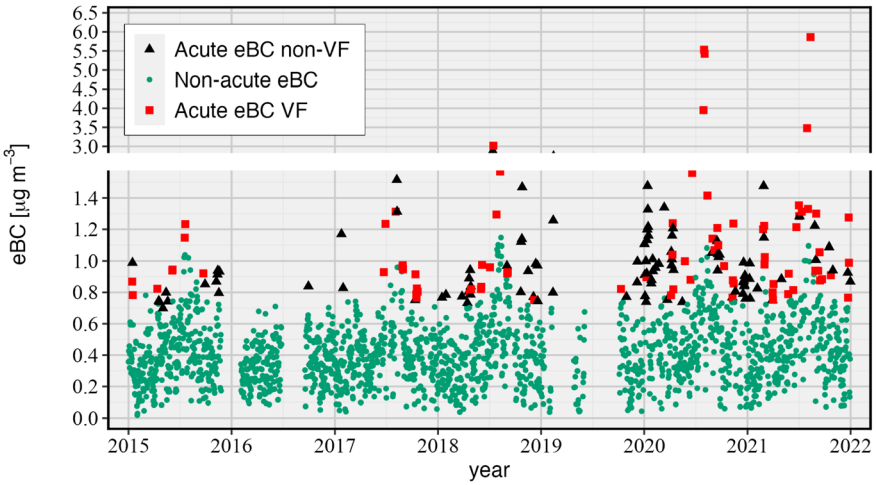

Fig. 3 Time series of daily eBC concentrations. Teal dots represent non-acute eBC days, black triangles indicate acute eBC days without vegetation fires (VF), and red squares denote acute eBC days with detected VF.

purposes in winter combined with occasional high-pressure episodes, which limit pollutant dispersion.[36–38] Nevertheless, this hypothesis was beyond the scope of the present study and was not further examined.

Considering only the acute days of eBC, we observe that the average annual eBC concentration was 1.17 ± 1.6 μg m^{-3}, which corresponds to over 200% of the background annual eBC concentration of 0.41 ± 0.45 μg m^{-3}, calculated by excluding the acute eBC days from the total population. Fig. 4, shows the annual variability of the eBC concentration over the entire period. The teal boxes are calculated from eBC daily averages excluding the acute eBC days, while the black triangles correspond to the eBC averages during acute eBC pollution days. To facilitate the interpretation of Fig. 4, a trend analysis was performed on acute eBC concentrations using the Theil–Sen estimator, which revealed a statistically significant increase of 0.04 μg m^{-3} year^{-1} (p-value < 0.05) across all acute eBC days. In terms of average seasonal concentration, the highest concentrations of acute eBC occur during summer (JJA, 1.75 ± 2.64 μg m^{-3}), which is nearly double compared to the other seasons (*e.g.*, DJF 0.99 ± 0.84 μg m^{-3}, MAM 0.92 ± 0.81 μg m^{-3}, and SON 0.87 ± 1.03 μg m^{-3}. This finding highlights the importance of further investigating biomass combustion-related events. While the frequency of acute eBC events is higher during the winter season, the same cannot be said for the intensity levels observed. The acute eBC days are characterized by daily average concentrations ranging from 0.70 to 5.86 μ g m^{-3} (February 1, 2015, and August 12, 2021, respectively), while all data without acute eBC days show averages varying between 0.02 and 1.3 μ g m^{-3}.

This is illustrated in Fig. 5, which presents the monthly and diurnal variations of non-acute eBC data after excluding acute days (teal line) compared to data from acute eBC days alone

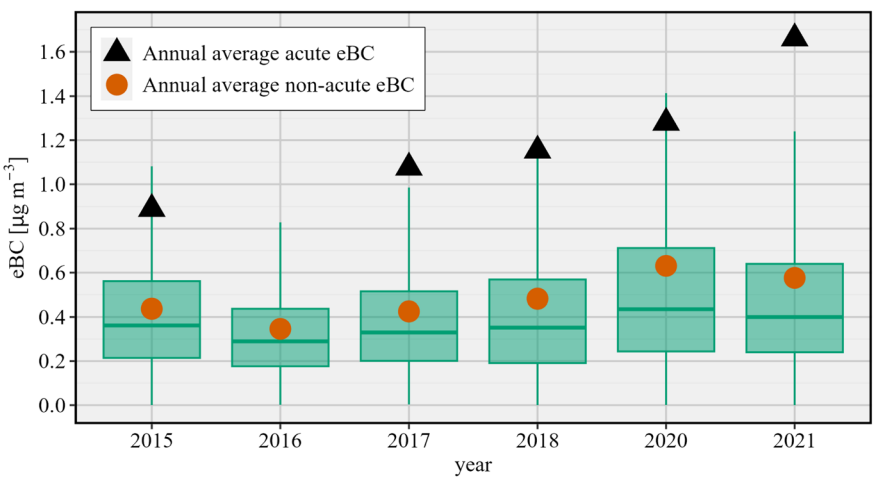

Fig. 4 Box plot of eBC concentration: teal green boxes represent non-acute eBC data; vermilion dots indicate the non-acute annual mean; black triangles indicate the mean eBC during acute days. For each year, the central line shows the median and the box spans the 25th–75th percentiles (interquartile range). Whiskers extend to the most extreme non-outlying values, and points beyond the whiskers are plotted as outliers.

Open Access Article. Published on 07 April 2026. Downloaded on 4/13/2026 10:22:05 AM.
This article is licensed under a Creative Commons Attribution-NonCommercial 3.0 Unported Licence.

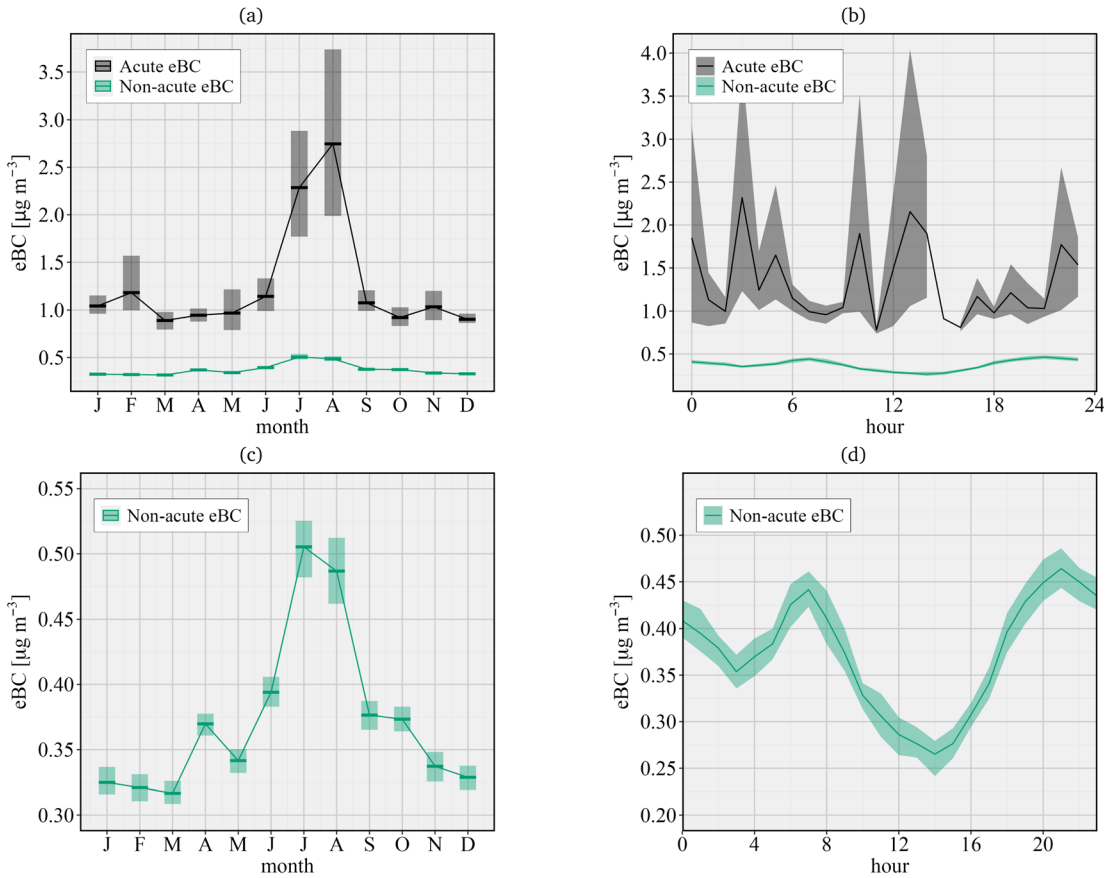

Fig. 5 Monthly (a) and diurnal (b) variations in eBC concentrations. Panels (c) and (d) provide zoomed-in views of (a) and (b), respectively, focusing on the contribution and variability of the non-acute eBC data. Shaded areas denote the 95% bootstrap confidence interval of the mean. Across all panels, non-acute eBC is shown in teal green and acute eBC in black.

(black line). Examining the latter, it is evident that no discernible pattern of daily variation exists, as acute events are random and lack cyclicality. Conversely, when acute eBC days are excluded, a distinct increase in eBC levels is observed in the morning (around 07 : 00 LT) and evening (around 21 : 00 LT),[18,39,40] consistent with the findings of Cristofanelli *et al.*, 2017.[37] Indeed, a preliminary assessment of local meteorology reveals that CGR is strongly influenced by a breeze regime. Nocturnal circulation is characterized by gentle land breezes (NW–NE, occurring 49% of the time), while sea breezes (W–SE) prevail during the day (80%). Regarding synoptic circulation, the site is predominantly affected by north-westerly air masses originating from the central Mediterranean basin.[37,41] This highlights that interactions between large-scale forcing patterns and local winds (*e.g.*, sea–land breezes) are important drivers of air quality dynamics and eBC variability.[42]

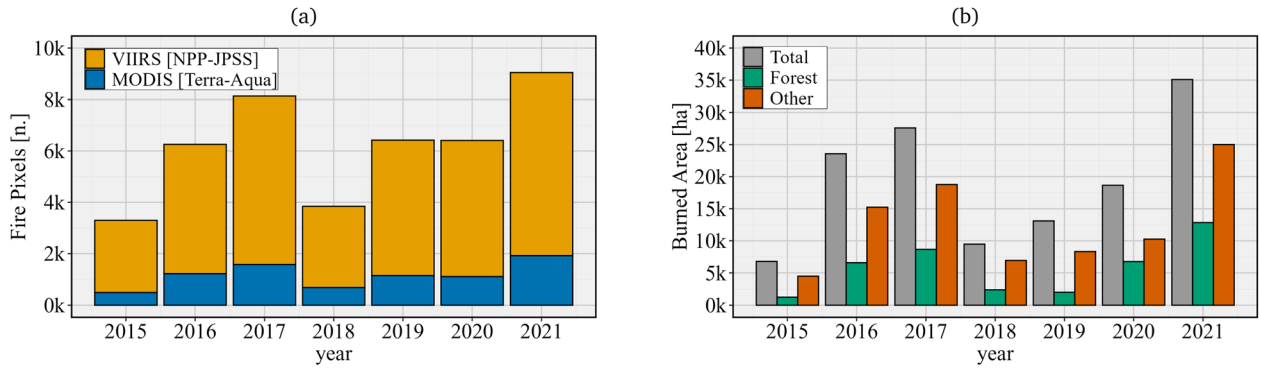

Fig. 6 (a) MODIS and VIIRS satellites: number of fire pixels (type = 0 – presumed vegetation) detected for the Sicily area. (b) Forest Information System (SIF): total burned area (grey), forest burned area (teal green), and other burned area (burnt orange).

© 2026 The Author(s). Published by the Royal Society of Chemistry

Open Access Article. Published on 07 April 2026. Downloaded on 4/13/2026 10:22:05 AM.
This article is licensed under a Creative Commons Attribution-NonCommercial 3.0 Unported Licence.

3.3 Influence of local vegetation fires

In recent years, the frequency of vegetation fires in the Mediterranean region has increased due to multiple climate change-related factors, including prolonged drought and rising temperatures.[43] In this region, fire emissions are an important contributor to the degradation of air quality, leading to increasing CO_2 emissions.[44] Consistent with this trend, Michetti and Pinar, 2019 (ref. 14), reported that 2017 was the year characterized by the largest number of fires in the past three decades in the Italian peninsula. Fig. 6 illustrates the annual trend of fire pixels detected by MODIS and VIIRS satellites within the region of interest (Section 2.1), alongside the total burned area reported by SIF. Based on these satellite observations, the highest frequency of fire pixels occurred in 2021 (9044) and 2017 (8132). To assess temporal patterns, a trend analysis was conducted using the Theil-Sen estimator, confirming a significant increase in vegetation fire frequency during the examined period. Specifically, the analysis reveals a robust upward trajectory for both sensors: VIIRS detects an average annual increase of approximately 683 fire pixels ($p = 0.015$), while MODIS indicates a consistent, albeit lower-magnitude, increase of 75 pixels per year ($p = 0.031$). Conversely, the average FRP remained statistically stable. This divergence suggests that the escalating impact on vegetation—reflected in the substantial burned area peaks observed in 2017 and 2021 (Fig. 6b)—is likely driven by a higher frequency of vegetation fire events rather than an increase in their individual intensity. During the study period, approximately 6330 vegetation fires were recorded in the region of interest, affecting about 135 000 hectares, of which approximately 30% were forested areas (averaging 6.1 kha year^{-1}) and

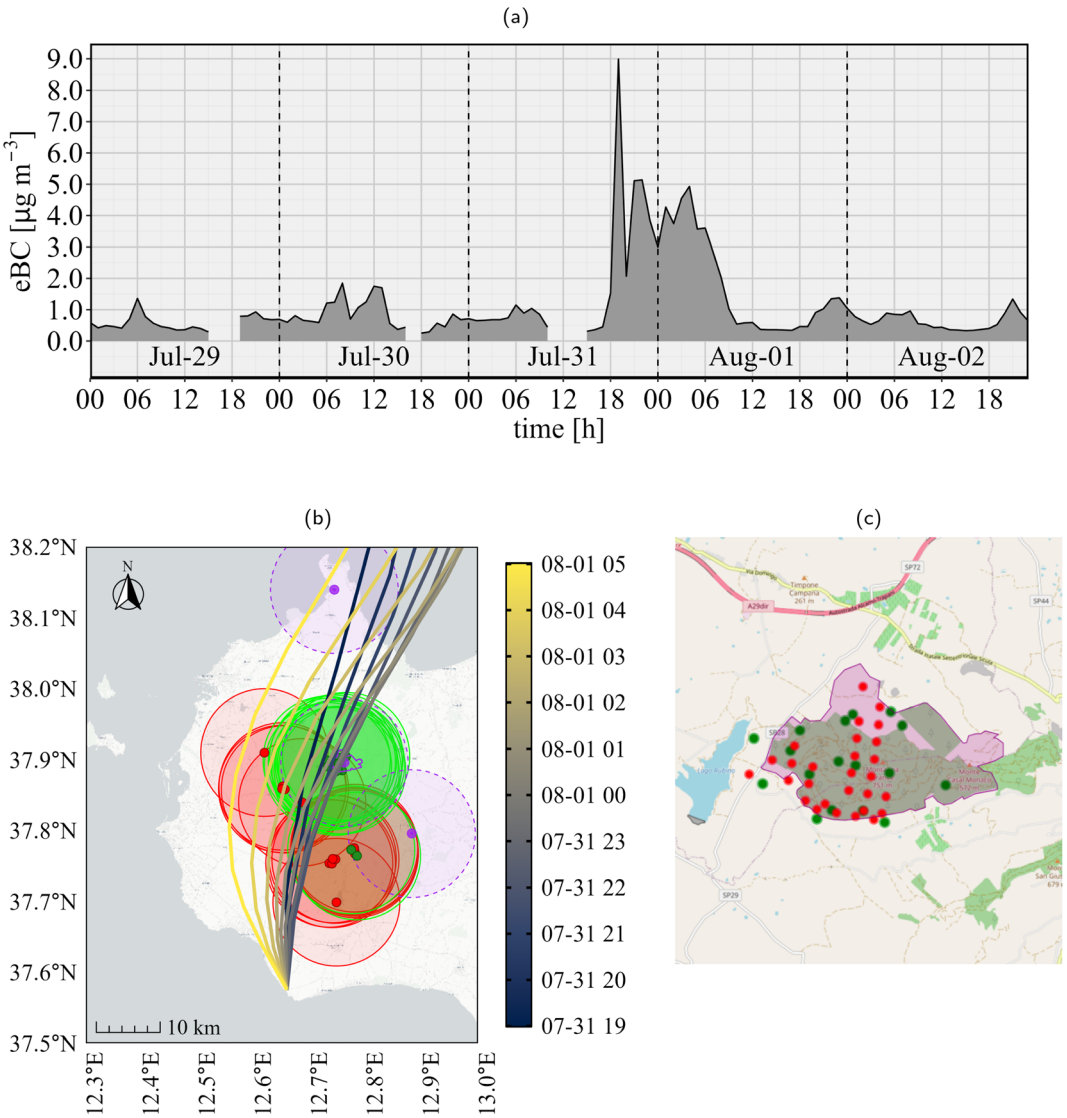

Fig. 7 Analysis of the Montagna Grande vegetation fire event on July 31st, 2020; (a) time series of the eBC concentration measured at CGR; (b) paths of back-trajectories with different start times (listed in the legend in month-day hour format [m-d h]) together with the identified fire pixels from MODIS (green dots), VIIRS (red dots), and SIF (purple dots); (c) fire pixel areas detected over Montagna Grande: MODIS (green dots), VIIRS (red dots), and the purple burned area identified by the SIF portal.

Open Access Article. Published on 07 April 2026. Downloaded on 4/13/2026 10:22:05 AM. This article is licensed under a Creative Commons Attribution-NonCommercial 3.0 Unported Licence.

67% were other types of land. Seasonally, 74% of these events occurred in summer, 18% in autumn, 7% in spring and only 1% in winter. These fires, through their widespread emissions and under specific meteorological conditions, can be transported on regional and continental scales, representing also a significant source of eBC. To quantify the impact of vegetation fires on the eBC concentration throughout the considered period (red squares in Fig. 3), we investigated the link between the 198 acute eBC days and vegetation fire data reported by satellite and SIF data (as described in Section 2.4). The key findings are summarized below:

• 91 (46%) of these acute eBC were linked to local vegetation fires detected by MODIS and VIIRS satellite products. Within this subset, the estimated Theil–Sen trend in eBC concentration was slightly lower (0.03 μg m^{-3} $year^{-1}$, p-value < 0.01) than the trend computed for all acute eBC days (0.04 μg m^{-3} $year^{-1}$), suggesting that the observed increase in acute eBC concentrations is not driven exclusively by the subset of acute days coincident with detected vegetation fires;

• On 3 days (1.5%), the back-trajectories passed through an SIF area without intersecting any satellite-detected fire pixels, indicating that fire pixels were not identified by the satellite;

• For the remaining 104 days (52.5%), the back-trajectories did not intersect any locally satellite-detected fire pixels or locally burned areas. Therefore, these acute eBC events cannot be explained by locally observed fire activity. In fact:

A significant portion of these days (68, corresponding to 65.4%) correspond to extra-regional events but were not explored because the goal of this work concerns regional contributions;

In the remaining cases (36, corresponding to 34.6%), no thermal anomalies were identified, and in some cases, the trajectories occurred entirely over the Mediterranean Sea. These acute eBC events occurred predominantly during winter (20, 59%), while only 2 events (6%) occurred in summer. This pattern likely reflects differences in the dynamics of the land–sea breeze system, suggesting a stronger influence of other sources and warranting further investigation.

4 Illustrative example: vegetation fire identification

Among all, the case of July 31st, 2020, was one of the most interesting. As can be seen from Fig. 7a, the anomalous event lasted approximately 17 hours (from July 31st at 17 : 00 to August 1st at 10 : 00 LT). In this period, the concentration of eBC reached the maximum value of 8.99 μg m^{-3} at 19 : 00 LT, with an average value of 13.46 ± 2.23 μg m^{-3}. During the considered event, several fires were detected by MODIS and VIIRS in the western part of Sicily and in particular around the green promontory of Montagna Grande (MG), which is about 36 km from CGR and extends over an area of almost 1300 ha, mainly characterized by pine trees, holm oaks, and downy oaks. This area extends over the municipalities of Trapani, Salemi, and Calatafimi, where the MODIS (green) and VIIRS (red) fire pixels active during this event were identified (Fig. 7b). During the considered case study, a total of 39 VIIRS fire pixels were recognized, of which 28 were concentrated in the MG area and 11 in other areas, while the MODIS satellite identified 17 fire pixels centered in the MG area. Based on the analysis of VIIRS metadata (at 00 : 50 LT on August 1st), the fire pixels associated with MG recorded an average Fire Radiative Power (FRP) value of 5.36, reaching a maximum of 9.3. In contrast, the FRP for fire pixels in other areas averaged 1.38, with a maximum of 2.0. Taking into account the 17 fire pixels detected in MG identified by MODIS, an average FRP value of 54.3, with a maximum of 444.2, was recorded. The transport of polluted air masses, rich in eBC emitted from the forest fires towards the southern coast of Sicily and the CGR observatory, was confirmed by the back-trajectories Fig. 7c) and the anticyclonic vortex over the Mediterranean-Sardinia region. Once emitted, the eBC levels measured at CGR depend on mechanical processes within the planetary boundary layer (PBL), which control dispersion and dilution.[45] This pattern indicates that the breeze regime was dominated by synoptic forcing, as shown by the MOLOCH model (see the CNR-ISAC website for further information). The analysis of the air mass transport, combined with information on forest fires that occurred in the area of MG, suggests that the acute eBC concentration registered at CGR can be attributed to emissions from forest and vegetation fires.

5 Conclusions

Through the combined analysis of air mass back-trajectories, satellite-derived fire detections (MODIS and VIIRS), ground-based SIF observations, and eBC measurements, we derived the following general conclusions:

• Of the 198 acute eBC days, only 94 were explained by local vegetation fire activity within the studied region. For the remaining 104 days, no satellite-detected thermal anomalies were identified in the regionally defined domain (see paragraph 2.1). In 68 of these days, extra-regional thermal anomalies were identified. This finding highlights the need to more thoroughly assess the contribution of extra-regional transport and/or non-fire combustion sources (*e.g.*, shipping emissions and residential heating) to observed eBC, particularly considering the CGR station's proximity to the Strait of Sicily and the high-density shipping lanes in the area.

• The mean eBC concentration measured at CGR over the study period (0.49 ± 0.69 μg m^{-3}) was comparable to values reported at other Mediterranean background and coastal sites, indicating that CGR reflects regional baseline conditions; consequently, these results provide a valuable evidence base for the scientific community and support the use of CGR as a representative reference site for future investigations of atmospheric transport, seasonality, and inter-annual variability in the central Mediterranean;

• During acute eBC days, the mean eBC concentration reaches 1.17 ± 1.6 μg m^{-3}, exceeding the annual baseline value (0.41 ± 0.45 μg m^{-3}) by more than 200%. This difference highlights how short-duration, highly concentrated episodes can dominate annual summary metrics, inflating mean and

 © 2026 The Author(s). Published by the Royal Society of Chemistry

Open Access Article. Published on 07 April 2026. Downloaded on 4/13/2026 10:22:05 AM.
This article is licensed under a Creative Commons Attribution-NonCommercial 3.0 Unported Licence.

variability, and thus masking underlying conditions that are more representative of the regional context;

• Local vegetation fires contributed to acute eBC concentrations at the CGR Observatory, as indicated by the subset of acute eBC events coincident with MODIS/VIIRS/SIF active-fire detections, which exhibits a statistically significant positive Theil–Sen trend over 2015–2021. However, the trend estimated for the vegetation fire-linked subset is slightly lower than the trend computed across all acute eBC days (Section 3.3), implying that the observed increase in acute eBC concentrations cannot be explained solely by the subset of events associated with detected local vegetation fires. Given known limitations of satellite active-fire products (*e.g.*, reduced detection capability under cloud/smoke obscuration, failure to detect smaller or less intense fires due to spatial resolution, or the lack of a coincident overflight due to the satellite's orbital trajectory and revisit time), and the persistence of a positive trend beyond the satellite-detected fire subset suggests that additional sources and processes (*e.g.*, anthropogenic combustion, regional transport, and meteorological variability) also contribute to acute eBC episodes,[46] underscoring the need for dedicated source-apportionment analyses to better separate vegetation-fire signals from other influences. Finally, the increase in the incidence/intensity of acute eBC events is significant not only for their negative impact on air quality, but also for the climate, given their significant positive radiative forcing;[8,47]

• The results highlight a statistically significant increase in the number of satellite-detected fire pixels within the defined domain, indicating that vegetation-fire occurrence in the region is becoming more frequent over the study period. This finding primarily reflects a change in the frequency and spatial extent of vegetation fires, rather than an increase in eBC concentrations at the CGR. When interpreted alongside the observed annual and seasonal variability of eBC at the CGR observatory, the increasing fire pixel trend provides policy-relevant evidence of a growing wildfire-related hazard in the central Mediterranean and motivates further work to quantify when and how these more frequent fire occurrences translate into measurable eBC impacts through transport and meteorological modulation.

Author contributions

Conceptualization: P. B., S. G., A. M., and S. S.; data curation: S. S., A. M., S. G., D. P., G. T., and L. D. L.; investigation: S. S., P. B., S. G., and A. M.; methodology: P. B., S. G., A. M., S. S., and T. C. L.; writing – original draft: S. S., P. B., and S. G.; writing – review and editing: S. S., P. B., S. G., D. P., and T. C. L.; project administration: P. B.

Conflicts of interest

The authors declare no conflicts of interest.

Data availability

The data used in this research are publicly accessible through established repositories and databases. Additional datasets presented or analyzed during the current study are available from the corresponding author on request.

Acknowledgements

We thank NASA for making FIRMS, MODIS and VIIRS data available to the scientific community. The HYSPLIT model is developed and provided by NOAA's Air Resource Laboratory. The SIF data are provided by the Forestry Corps of the Sicilian Region. The authors would like to thank G. Pavese for useful suggestions during the writing session and G. Verrazzo for technical support during code writing.

References

1 Intergovernmental Panel on Climate Change (IPCC), in *Climate Change 2021 - the Physical Science Basis*, Cambridge University Press, 2023, pp. 35–144, DOI: 10.1017/9781009157896.002.

2 N. A. Janssen, G. Hoek, M. Simic-Lawson, P. Fischer, L. van Bree, H. ten Brink, M. Keuken, R. W. Atkinson, H. R. Anderson, B. Brunekreef and F. R. Cassee, Black Carbon as an Additional Indicator of the Adverse Health Effects of Airborne Particles Compared with PM10 and PM2.5, *Environ. Health Perspect.*, 2011, **119**, 1691–1699, DOI: 10.1289/ehp.1003369.

3 D. Koch, M. Schulz, S. Kinne, C. McNaughton, J. R. Spackman, Y. Balkanski, S. Bauer, T. Berntsen, T. C. Bond, O. Boucher, M. Chin, A. Clarke, N. De Luca, F. Dentener, T. Diehl, O. Dubovik, R. Easter, D. W. Fahey, J. Feichter, D. Fillmore, S. Freitag, S. Ghan, P. Ginoux, S. Gong, L. Horowitz, T. Iversen, Kirkev&aring, A. G. Z. Klimont, Y. Kondo, M. Krol, X. Liu, R. Miller, V. Montanaro, N. Moteki, G. Myhre, J. E. Penner, J. Perlwitz, G. Pitari, S. Reddy, L. Sahu, H. Sakamoto, G. Schuster, J. P. Schwarz, Ã. Seland, P. Stier, N. Takegawa, T. Takemura, C. Textor, J. A. van Aardenne and Y. Zhao, Evaluation of black carbon estimations in global aerosol models, *Atmos. Chem. Phys.*, 2009, **9**, 9001–9026, DOI: 10.5194/acp-9-9001-2009.

4 T. C. Bond and R. W. Bergstrom, Light Absorption by Carbonaceous Particles: An Investigative Review, *Aerosol Sci. Technol.*, 2006, **40**, 27–67, DOI: 10.1080/02786820500421521.

5 W. Li, P. Ge, M. Chen, J. Tang, M. Cao, Y. Cui, K. Hu and D. Nie, Tracers from Biomass Burning Emissions and Identification of Biomass Burning, *Atmosphere*, 2021, **12**, 1401, DOI: 10.3390/atmos12111401.

6 J. N. Cape, M. Coyle and P. Dumitrean, The atmospheric lifetime of black carbon, *Atmos. Environ.*, 2012, **59**, 256–263, DOI: 10.1016/j.atmosenv.2012.05.030.

7 I. L. Karol', A. A. Kiselev, E. L. Genikhovich and S. S. Chicherin, Reduction of short-lived atmospheric pollutant emissions as an alternative strategy for climate-change moderation, *Izv. Atmos. Ocean. Phys.*, 2013, **49**, 461–478, DOI: 10.1134/S0001433813050058.

Open Access Article. Published on 07 April 2026. Downloaded on 4/13/2026 10:22:05 AM. This article is licensed under a Creative Commons Attribution-NonCommercial 3.0 Unported Licence.

8 T. C. Bond, S. J. Doherty, D. W. Fahey, P. M. Forster, T. Berntsen, B. J. DeAngelo, M. G. Flanner, S. Ghan, B. Kärcher, D. Koch, S. Kinne, Y. Kondo, P. K. Quinn, M. C. Sarofim, M. G. Schultz, M. Schulz, C. Venkataraman, H. Zhang, S. Zhang, N. Bellouin, S. K. Guttikunda, P. K. Hopke, M. Z. Jacobson, J. W. Kaiser, Z. Klimont, U. Lohmann, J. P. Schwarz, D. Shindell, T. Storelvmo, S. G. Warren and C. S. Zender, Bounding the role of black carbon in the climate system: A scientific assessment, *J. Geophys. Res. Atmos.*, 2013, **118**, 5380–5552, DOI: 10.1002/jgrd.50171.

9 T. C. Bond, D. G. Streets, K. F. Yarber, S. M. Nelson, J. Woo and Z. Klimont, A technology-based global inventory of black and organic carbon emissions from combustion, *J. Geophys. Res. Atmos.*, 2004, **109**, 2003JD003697, DOI: 10.1029/2003JD003697.

10 Y. Liu, S. L. Goodrick and J. A. Stanturf, Future U.S. wildfire potential trends projected using a dynamically downscaled climate change scenario, *For. Ecol. Manag.*, 2013, **294**, 120–135, DOI: 10.1016/j.foreco.2012.06.049.

11 D. McKenzie, U. Shankar, R. E. Keane, E. N. Stavros, W. E. Heilman, D. G. Fox and A. C. Riebau, Smoke consequences of new wildfire regimes driven by climate change, *Earths Future*, 2014, **2**, 35–59, DOI: 10.1002/2013EF000180.

12 A. Veira, G. Lasslop and S. Kloster, Wildfires in a warmer climate: Emission fluxes, emission heights, and black carbon concentrations in 2090-2099, *J. Geophys. Res. Atmos.*, 2016, **121**, 3195–3223, DOI: 10.1002/2015JD024142.

13 A. Ganteaume, R. Barbero, M. Jappiot and E. Maillé, Understanding future changes to fires in southern Europe and their impacts on the wildland-urban interface, *J. Saf. Sci. Resil.*, 2021, **2**, 20–29, DOI: 10.1016/j.jnlssr.2021.01.001.

14 M. Michetti and M. Pinar, Forest Fires Across Italian Regions and Implications for Climate Change: A Panel Data Analysis, *Environ. Resour. Econ.*, 2019, **72**, 207–246, DOI: 10.1007/s10640-018-0279-z.

15 M. Mallet, O. Dubovik, P. Nabat, F. Dulac, R. Kahn, J. Sciare, D. Paronis and J. F. Léon, Absorption properties of Mediterranean aerosols obtained from multi-year ground-based remote sensing observations, *Atmos. Chem. Phys.*, 2013, **13**, 9195–9210, DOI: 10.5194/acp-13-9195-2013.

16 L. V. Noto, G. Cipolla, A. Francipane and D. Pumo, Climate Change in the Mediterranean Basin (Part I): Induced Alterations on Climate Forcings and Hydrological Processes, *Water Resour. Manag.*, 2023, **37**, 2287–2305, DOI: 10.1007/s11269-022-03400-0.

17 L. Naitza, D. Putero, A. Marinoni, F. Calzolari, F. Roccato, M. Busetto, D. Sferlazzo, E. Aruffo, P. Carlo, M. Bencardino, F. D'Amore, F. Sprovieri, N. Pirrone, F. Dallo, J. Gabrieli, M. Varde, C. Barbante, P. Bonasoni and P. Cristofanelli, Automatic procedures for submitting essential climate variables (ECVs) recorded at Italian Atmospheric Observatories to WMO/GAW data centers, *Atmos. Meas. Tech. Discuss.*, 2018, 1–22, DOI: 10.5194/amt-2018-245.

18 L. A. Remer, R. G. Kleidman, R. C. Levy, Y. J. Kaufman, D. Tanré, S. Mattoo, J. V. Martins, C. Ichoku, I. Koren, H. Yu and B. N. Holben, Global aerosol climatology from the MODIS satellite sensors, *J. Geophys. Res.*, 2008, **113**, 2007JD009661, DOI: 10.1029/2007JD009661.

19 L. Giglio, W. Schroeder and C. O. Justice, The collection 6 MODIS active fire detection algorithm and fire products, *Rem. Sens. Environ.*, 2016, **178**, 31–41, DOI: 10.1016/j.rse.2016.02.054.

20 W. Schroeder, P. Oliva, L. Giglio and I. A. Csiszar, The New VIIRS 375 m active fire detection data product: Algorithm description and initial assessment, *Rem. Sens. Environ.*, 2014, **143**, 85–96, DOI: 10.1016/j.rse.2013.12.008.

21 A. F. Stein, R. R. Draxler, G. D. Rolph, B. J. B. Stunder, M. D. Cohen and F. Ngan, NOAA's HYSPLIT Atmospheric Transport and Dispersion Modeling System, *Bull. Am. Meteorol. Soc.*, 2015, **96**, 2059–2077, DOI: 10.1175/BAMS-D-14-00110.1.

22 L. Su, Z. Yuan, J. C. Fung and A. K. Lau, A comparison of HYSPLIT backward trajectories generated from two GDAS datasets, *Sci. Total Environ.*, 2015, **506–507**, 527–537, DOI: 10.1016/j.scitotenv.2014.11.072.

23 P. Malguzzi, G. Grossi, A. Buzzi, R. Ranzi and R. Buizza, The 1966 "century" flood in Italy: A meteorological and hydrological revisitation, *J. Geophys. Res. Atmos.*, 2006, **111**, year, DOI: 10.1029/2006JD007111.

24 A. Marinoni, P. Cristofanelli, P. Laj, R. Duchi, D. Putero, F. Calzolari, T. Landi, E. Vuillermoz, M. Maione and P. Bonasoni, High black carbon and ozone concentrations during pollution transport in the Himalayas: Five years of continuous observations at NCO-P global GAW station, *J. Environ. Sci.*, 2013, **25**, 1618–1625, DOI: 10.1016/S1001-0742(12)60242-3.

25 P. Laj, A. Bigi, C. Rose, E. Andrews, C. Lund Myhre, M. Collaud Coen, Y. Lin, A. Wiedensohler, M. Schulz, J. A. Ogren, M. Fiebig, J. GliÃŸ, A. Mortier, M. Pandolfi, T. Petäja, S.-W. Kim, W. Aas, J.-P. Putaud, O. Mayol-Bracero, M. Keywood, L. Labrador, P. Aalto, E. Ahlberg, L. Alados Arboledas, A. Alastuey, M. Andrade, B. Artíñano, S. Ausmeel, T. Arsov, E. Asmi, J. Backman, U. Baltensperger, S. Bastian, O. Bath, J. P. Beukes, B. T. Brem, N. Bukowiecki, S. Conil, C. Couret, D. Day, W. Dayantolis, A. Degorska, K. Eleftheriadis, P. Fetfatzis, O. Favez, H. Flentje, M. I. Gini, A. Gregorič, M. Gysel-Beer, A. G. Hallar, J. Hand, A. Hoffer, C. Hueglin, R. K. Hooda, A. Hyvärinen, I. Kalapov, N. Kalivitis, A. Kasper-Giebl, J. E. Kim, G. Kouvarakis, I. Kranjc, R. Krejci, M. Kulmala, C. Labuschagne, H.-J. Lee, H. Lihavainen, N.-H. Lin, G. Löschau, K. Luoma, A. Marinoni, S. Martins Dos Santos, F. Meinhardt, M. Merkel, J.-M. Metzger, N. Mihalopoulos, N. A. Nguyen, J. Ondracek, N. Pérez, M. R. Perrone, J.-E. Petit, D. Picard, J.-M. Pichon, V. Pont, N. Prats, A. Prenni, F. Reisen, S. Romano, K. Sellegri, S. Sharma, G. Schauer, P. Sheridan, J. P. Sherman, M. Schütze, A. Schwerin, R. Sohmer, M. Sorribas, M. Steinbacher, J. Sun, G. Titos, B. Toczko, T. Tuch, P. Tulet, P. Tunved, V. Vakkari, F. Velarde, P. Velasquez, P. Villani, S. Vratolis,

 © 2026 The Author(s). Published by the Royal Society of Chemistry

Open Access Article. Published on 07 April 2026. Downloaded on 4/13/2026 10:22:05 AM. This article is licensed under a Creative Commons Attribution-NonCommercial 3.0 Unported Licence.

S.-H. Wang, K. Weinhold, R. Weller, M. Yela, J. Yus-Diez, V. Zdimal, P. Zieger and N. Zikova, A global analysis of climate-relevant aerosol properties retrieved from the network of Global Atmosphere Watch (GAW) near-surface observatories, *Atmos. Meas. Tech.*, 2020, **13**, 4353–4392, DOI: 10.5194/amt-13-4353-2020.

26 D. Putero, T. Landi, P. Cristofanelli, A. Marinoni, P. Laj, R. Duchi, F. Calzolari, G. Verza and P. Bonasoni, Influence of open vegetation fires on black carbon and ozone variability in the southern Himalayas (NCO-P, 5079 m a.s.l.), *Environ. Pollut.*, 2014, **184**, 597–604, DOI: 10.1016/j.envpol.2013.09.035.

27 H. Theil, *A Rank-Invariant Method of Linear and Polynomial Regression Analysis*, 1950, vol. III 1.

28 P. Kumar Sen, ESTIMATES OF THE REGRESSION COEFFICIENT BASED ON KENDALL'S TAU, *J. Am. Stat. Assoc.*, 1968, **63**(324), 1379–1389.

29 C. Rose, M. Collaud Coen, E. Andrews, Y. Lin, I. Bossert, C. Lund Myhre, T. Tuch, A. Wiedensohler, M. Fiebig, P. Aalto, A. Alastuey, E. Alonso-Blanco, M. Andrade, B. Artíñano, T. Arsov, U. Baltensperger, S. Bastian, O. Bath, J. P. Beukes, B. T. Brem, N. Bukowiecki, J. A. Casquero-Vera, S. Conil, K. Eleftheriadis, O. Favez, H. Flentje, M. I. Gini, F. J. Gómez-Moreno, M. Gysel-Beer, A. G. Hallar, I. Kalapov, N. Kalivitis, A. Kasper-Giebl, M. Keywood, J. E. Kim, S.-W. Kim, A. Kristensson, M. Kulmala, H. Lihavainen, N.-H. Lin, H. Lyamani, A. Marinoni, S. Martins Dos Santos, O. L. Mayol-Bracero, F. Meinhardt, M. Merkel, J.-M. Metzger, N. Mihalopoulos, J. Ondracek, M. Pandolfi, N. Pérez, T. Petäjä, J.-E. Petit, D. Picard, J.-M. Pichon, V. Pont, J.-P. Putaud, F. Reisen, K. Sellegri, S. Sharma, G. Schauer, P. Sheridan, J. P. Sherman, A. Schwerin, R. Sohmer, M. Sorribas, J. Sun, P. Tulet, V. Vakkari, P. G. van Zyl, F. Velarde, P. Villani, S. Vratolis, Z. Wagner, S.-H. Wang, K. Weinhold, R. Weller, M. Yela, V. Zdimal and P. Laj, Seasonality of the particle number concentration and size distribution: a global analysis retrieved from the network of Global Atmosphere Watch (GAW) near-surface observatories, *Atmos. Chem. Phys.*, 2021, **21**, 17185–17223, DOI: 10.5194/acp-21-17185-2021.

30 D. C. Hoaglin, L. Dümbgen and H. Riedwyl, On fences and asymmetry in box-and-whiskers plots, *Am. Statistician*, 2008, **62**, 187, DOI: 10.1198/000313008X306376.

31 A. Saha and S. Despiau, Seasonal and diurnal variations of black carbon aerosols over a Mediterranean coastal zone, *Atmos. Res.*, 2009, **92**, 27–41, DOI: 10.1016/j.atmosres.2008.07.007.

32 M. Zanatta, M. Gysel, N. Bukowiecki, T. Müller, E. Weingartner, H. Areskoug, M. Fiebig, K. E. Yttri, N. Mihalopoulos, G. Kouvarakis, D. Beddows, R. M. Harrison, F. Cavalli, J. P. Putaud, G. Spindler, A. Wiedensohler, A. Alastuey, M. Pandolfi, K. Sellegri, E. Swietlicki, J. L. Jaffrezo, U. Baltensperger and P. Laj, A European aerosol phenomenology-5: Climatology of black carbon optical properties at 9 regional background sites across Europe, *Atmos. Environ.*, 2016, **145**, 346–364, DOI: 10.1016/J.ATMOSENV.2016.09.035.

33 A. Donateo, T. Lo Feudo, A. Marinoni, C. R. Calidonna, D. Contini and P. Bonasoni, Long-term observations of aerosol optical properties at three GAW regional sites in the Central Mediterranean, *Atmos. Res.*, 2020, **241**, 104976, DOI: 10.1016/j.atmosres.2020.104976.

34 A. Milinković, A. Gregorič, V. D. Grgičin, S. Vidič, A. Penezić, A. C. Kušan, S. B. Alempijević, A. Kasper-Giebl and S. Frka, Variability of black carbon aerosol concentrations and sources at a Mediterranean coastal region, *Atmos. Pollut. Res.*, 2021, **12**, 101221, DOI: 10.1016/j.apr.2021.101221.

35 V. Matos, V. Estellés, J. Camarasa, M. Sorribas and M. P. Utrillas, Characterization of equivalent Black Carbon (eBC) in different environments in the western Mediterranean, *Atmos. Pollut. Res.*, 2025, **16**, 102367, DOI: 10.1016/j.apr.2024.102367.

36 J. Krynicka and A. Drzeniecka-Osiadacz, *Analysis of Variability in PM10 Concentration in the Wrocław Agglomeration*, 2013.

37 P. Cristofanelli, M. Busetto, F. Calzolari, I. Ammoscato, D. Gullì, A. Dinoi, C. R. Calidonna, D. Contini, D. Sferlazzo, T. Di Iorio, S. Piacentino, A. Marinoni, M. Maione and P. Bonasoni, Investigation of reactive gases and methane variability in the coastal boundary layer of the central Mediterranean basin, *Elementa: Sci. Anthropocene.*, 2017, **5**, 12, DOI: 10.1525/elementa.216.

38 M. Gorka, E. Kosztowniak, A. U. Lewandowska and D. Widory, Carbon isotope compositions and TC/OC/EC levels in atmospheric PM10 from Lower Silesia (SW Poland): Spatial variations, seasonality, sources and implications, *Atmos. Pollut. Res.*, 2020, **11**, 1099–1114, DOI: 10.1016/j.apr.2020.04.003.

39 J. Crawford, A. Griffiths, D. D. Cohen, N. Jiang and E. Stelcer, Particulate Pollution in the Sydney Region: Source Diagnostics and Synoptic Controls, *Aerosol Air Qual. Res.*, 2016, **16**, 1055–1066, DOI: 10.4209/aaqr.2015.02.0081.

40 M. A. Storey and O. F. Price, Prediction of air quality in Sydney, Australia as a function of forest fire load and weather using Bayesian statistics, *PLoS One*, 2022, **17**, e0272774, DOI: 10.1371/journal.pone.0272774.

41 M. Rinaldi, A. Nicosia, G. Santachiara, M. Piazza, M. Paglione, S. Gilardoni, S. Sandrini, P. Cristofanelli, A. Marinoni, P. Bonasoni, M. C. Facchini and F. Belosi, Ground level ice nucleating particles measurements at Capo Granitola, a Mediterranean coastal site, *Atmos. Res.*, 2019, **219**, 57–64, DOI: 10.1016/J.ATMOSRES.2018.12.022.

42 S. Federico, L. Pasqualoni, A. M. Sempreviva, L. De Leo, E. Avolio, C. R. Calidonna and C. Bellecci, The seasonal characteristics of the breeze circulation at a coastal Mediterranean site in South Italy, *Adv. Sci. Res.*, 2010, **4**, 47–56, DOI: 10.5194/ASR-4-47-2010.

43 T. Hiraishi, T. Krug, K. Tanabe, N. Srivastava, B. Jamsranjav, M. Fukuda and T. Troxler, *Revised Supplementary Methods and Good Practice Guidance Arising from the Kyoto Protocol*, Intergovernmental Panel on Climate Change, 2014.

44 R. Silvestro, L. Saulino, C. Cavallo, E. Allevato, S. Pindozzi, E. Cervelli, P. Conti, S. Mazzoleni and A. Saracino, The Footprint of Wildfires on Mediterranean Forest Ecosystem

Open Access Article. Published on 07 April 2026. Downloaded on 4/13/2026 10:22:05 AM.
This article is licensed under a Creative Commons Attribution-NonCommercial 3.0 Unported Licence.

Services in Vesuvius National Park, *Fire*, 2021, **4**, 95, DOI: 10.3390/fire4040095.

45 Y. Miao, H. Che, X. Zhang and S. Liu, Integrated impacts of synoptic forcing and aerosol radiative effect on boundary layer and pollution in the Beijing-Tianjin-Hebei region, China, *Atmos. Chem. Phys.*, 2020, **20**, 5899–5909, DOI: 10.5194/acp-20-5899-2020.

46 M. Viana, P. Hammingh, A. Colette, X. Querol, B. Degraeuwe, I. d. Vlieger and J. van Aardenne, Impact of maritime transport emissions on coastal air quality in Europe, *Atmos. Environ.*, 2014, **90**, 96–105, DOI: 10.1016/J.ATMOSENV.2014.03.046.

47 V. Ramanathan and G. Carmichael, Global and regional climate changes due to black carbon, *Nat. Geosci.*, 2008, **1**, 221–227, DOI: 10.1038/NGEO156.

© 2026 The Author(s). Published by the Royal Society of Chemistry